Low-cost bilayered structure for improving the performance of solar stills: Performance/cost analysis and water yield prediction using machine learning

Ammar H. Elsheikh [a,*], S. Shanmugan [b], Ravishankar Sathyamurthy [c], Amrit Kumar Thakur [d], Mohamed Issa [e], Hitesh Panchal [f], T. Muthuramalingam [g], Ravinder Kumar [h,*], Mohsen Sharifpur [i,j,*]

[a] Department of Mechanical Design, Faculty of Engineering, Tanta University, Tanta 31527, Egypt
[b] Research Centre for Solar Energy, Koneru Lakshmaiah Education Foundation, Green Fields, Guntur District, Vaddeswaram, Andhra Pradesh 522502, India
[c] Department of Mechanical Engineering, KPR Institute of Engineering and Technology, Coimbatore 641 407, Tamil Nadu, India
[d] Department of Mechanical Engineering, KPR Institute Engineering and Technology, Coimbatore, Tamil Nadu, India
[e] Computer and Systems Department, Faculty of Engineering, Zagazig University, Egypt
[f] Department of Mechanical Engineering, Government Engineering College, Patan, Gujarat, India
[g] Department of Mechatronics Engineering, Kattankulathur Campus, SRM Institute of Science and Technology, Chennai 603203, India
[h] Department of Mechanical Engineering, Lovely Professional University, Phagwara, Jalandhar 144411, Punjab, India
[i] Clean Energy Research Group, Department of Mechanical and Aeronautical Engineering, University of Pretoria, Hatfield, Pretoria, South Africa
[j] Department of Medical Research, China Medical University Hospital, China Medical University, Taichung, Taiwan

A R T I C L E I N F O

Keywords:
Low cost materials
Water desalination
Solar energy
Solar still
Heat localization
Machine learning

A B S T R A C T

This paper aims to enhance the performance of conventional solar still (CSS) using a low cost heat localization bilayered structure (HLBS). The HLBS consists of a bottom supporting layer (SL) made of low thermal conductivity as well as low density material and a top absorbing layer (AL) made of a photo thermal material with a high sunlight absorptivity as well as an enhanced conversion efficiency. The developed HLBS helps in increasing the evaporation rate and minimize the heat losses in a modified solar still (MSS). Two similar SSs were designed and tested to evaluate SSs' performance without and with HLBS (CSS and MSS). Moreover, three machine learning (ML) methods were utilized as predictive tools to obtain the water yield of the SSs, namely artificial neural network (ANN), support vector machine (SVM), and adaptive neuro-fuzzy inference system (ANFIS). The prediction accuracy of the models was evaluated using different statistical measured. The obtained results showed that the daily freshwater yield, energy efficiency, and exergy efficiency of the MSS was enhanced by 34%, 34%, and 46% compared with that of CSS. The production cost per liter of the MSS is 0.015 $/L. Moreover, SVM outperformed other ML methods for both SSs based on different statistical measures.

Introduction

Freshwater is a fundamental human need. Water covers about 70% of the surface of the Earth (1386 × 10^{33} m^3) [77]. Unfortunately, only 0.5% of total global water is freshwater which stored in rivers and lakes, while about 97.5% of it exists in the oceans and seas with high salinity and the remaining amount (about 2%) exists in the form of glaciers and groundwater [6]. The rapid population growth, as well as astonishing economic growth, increases the request of the freshwater [13,87,100] with minimum environmental impacts [98,103]. There are many methods used for water desalination such as multi-stage flash distillation [88], vapor-compression distillation[75], reverse osmosis[106], membrane distillation[12], halophytic algae[82], multi effect distillation [74], vacuum membrane[111], electrodialysis membrane[11], wave-powered desalination[60], solar chimneys[2], and solar desalination [95].

Solar desalination has shown promising applications in obtaining freshwater from seawater. Solar stills (SSs) is one of the most common used solar desalination systems that characterized by low cost, simple in

* Corresponding authors.
E-mail addresses: ammar_elsheikh@f-eng.tanta.edu.eg (A.H. Elsheikh), Mamohamedali@eng.zu.edu.eg (M. Issa), rav.chauhan@yahoo.co.in (R. Kumar), mohsen.sharifpur@up.ac.za (M. Sharifpur).

Nomenclature

A_b	basin area (m^2)	ML	Machine learning
ANFIS	Adaptive neuro-fuzzy inference system	MRE	Mean relative error
AL	Absorbing layer	MSS	Modified solar still
AMC	Annual maintenance operational cost	n	Number of variables
ANN	Artificial neural network	OI	Overall index
ASV	Annual salvage value	P	Petela
c	Bias	R	Response
COV	Coefficient of variation	RMSE	Root mean square error
CPL	Cost of distilled water per liter	R^2	Coefficient of determination
CRF	Capital recovery factor	SFF	Sinking fund factor
CSS	Conventional solar still	S	Salvage value
E_{ev}	Exergy of evaporation (J)	SL	supporting layer
E_{ir}	Exergy of solar irradiance (J)	SS	Solar still
EC	Efficiency coefficient	SVM	Support vector machine
$f_i(x)$	Nonlinear transformation function	T_w	water temperature (K)
HLBS	Heat localization bilayered structure	T_a	ambient temperature (K)
i	Interest per year (%)	T_s	Sun temperature
i(t)	Solar radiation(W/m^2)	U_R	Response uncertainty
L	Latent heat of evaporation(J/kg)	x	Training set
M	Annual yield (l)	X	Input variable
MAE	Mean absolute error	ε_i	Weights
		ηeh	Hourly energy efficiency
		Γ	Kernel function

Table 1
A summary of different heat localization structures investigated in literature.

References	Absorbing layer	Supporting layer
[41]	Exfoliated graphite	Carbon foam
[68]	Carbon black	Cotton gauze
[112]	Graphene	Nanoporous Ni substrates
[110]	Gold	Air-laid paper
[114]	Gold	Aluminum oxide
[8]	Gold	Microporous membrane
[64]	Polypyrrole	Stainless steel mesh
[62]	Graphene oxide	Cellulose over polystyrene foam
[79]	Graphene oxide	Bacterial nanocellulose
[118]	Aluminum	Anodic aluminum oxide
[119]	Titanium dioxide	Nanocage structure
[73]	Cermet	Copper sheet
[55]	Graphite flakes and carbon fibers	Polymer skeleton
[63]	Graphene oxide/carbon black	Polystyrene matrix
[105]	Gold	Treated paper
[47]	Gold/titanium dioxide	Polymeric membrane
[38]	Silver/diatomite	Paper attached to polystyrene foam
[65]	Graphene oxide	Wood
[109]	Carbon	Wood
[108]	Polydopamine	Wood
[56]	Titanium nitride	Ceramic fiber wools
[44]	Titanium dioxide	Cotton fabric
[45]	Titanium dioxide	Carbon fabric
[67]	Black titania/graphene oxide	Air-laid paper
[61]	Graphite	Wood
[117]	Copper sulfide	Cellulose ester membrane
[69]	Carbon particles	Cellulose sponge
[49]	Carbon particles	Attapulgite/poly acrylamide composite
[70]	Carbon particles	Paper attached to polyethylene
[96]	Copper sulfide	Macroporous polyacrylamide hydrogel
[66]	Carbon particles	Sawdust film
[17]	Jute	Plastic balls
[116]	Chinese ink	Wood

operation, and easy to maintain[86]). In SSs, solar radiation is utilized as a heat source to heat up brackish water which consequently begins to evaporate leaving contaminants and salts in the basin, and then the evaporated water cools down on the inner surface of glazier cover and condenses into liquid water droplets which collected as a pure water. The main drawback of SSs is its low freshwater productivity. Therefore, there are continued hard efforts done by many scientists and researchers to improve productivity and thermal performance of SSs via applying different designs such as passive SS, active SS[40], double slope SS[83], inclined SS[76,85], weir type SS[4], pyramid SS [53], and tubular SS [89]. Moreover, different modifications and integrations with SS such as solar water heater[9], photovoltaic panel[22], glass cover cooling [31,94], heat storage system[113], nanofluids[32,92], organic colloids [35], solar dishes[52], parabolic concentrating solar collector[3], external flat-plate reflectors[57], hybrid wick/chip materials[90], external condenser[80], permanent magnets[18], nano-composite materials[37], heat localization devices[93], solar pond[16], enhanced absorber plate[50], enhanced condensation surface[107], and underground heat exchanger[43]have been investigated.

Recently, heat localization devices that used to enhance the solar energy harvesting via heating up a thin layer of water instead of bulk water have attracted the attention of many researchers[30]. Heat localization devices are composed of an AL which has high sunlight absorptivity and high conversion efficiency to enhance the solar energy harvesting and a SL which used as a carrier to the AL and as an insulation layer to confine heat in the AL. The SL should be made of low density material. The heat localization device should also be made of low cost easy to fabricate material which characterized by a reasonable scalability and durability. A summary of different AL and SL materials investigated in literature are tabulated in Table 1. However, most of studies listed in this table have been conducted in laboratories under artificial sunlight produced by solar simulator. Therefore, more experimental investigations on the application of these heat localization bilayered structures in SSs under real world conditions should be done.

Modeling of SSs using conventional mathematical approaches is a cumbersome problem which requires many assumptions to simplify the real-world system [1]. Therefore, ML approaches have been proposed as accurate and reliable modeling techniques of different solar systems including SS [29,59,72]. The distillate production of a CSS was predicted using an ML model under the metrological data of Las Vegas, USA using different parameters such a, air temperature, air velocity and direction and cloud cover [84]. The performance of the SS was

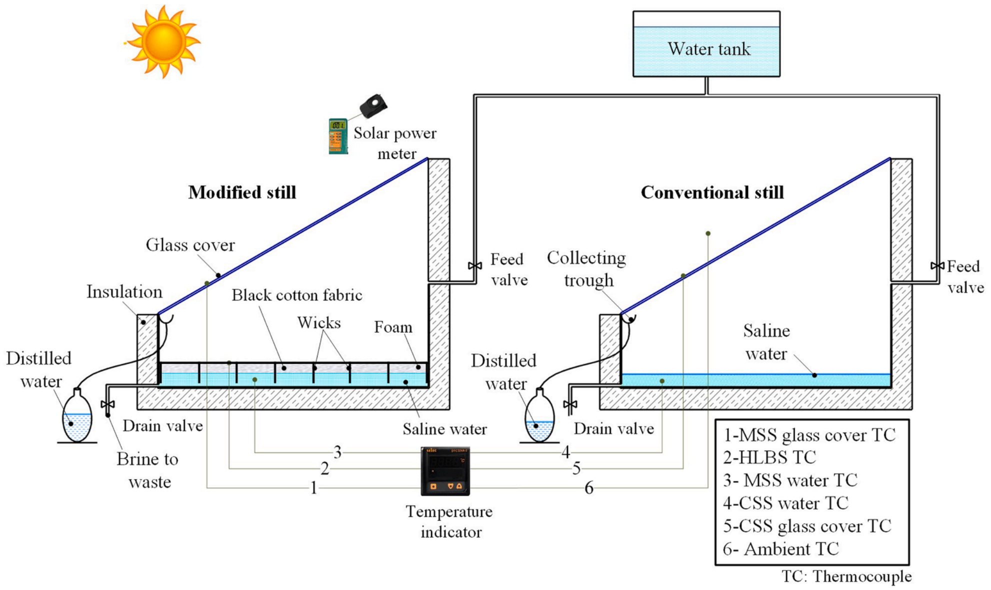

Fig. 1. Experimental set up.

successfully predicted using the proposed model at various operating conditions. In another study, three ML models were established to predict the water yield of a SS under the metrological data of Jordan [42]. Feed-forward neural network outperformed the other models. [71] used an ANN predictive model to predict the water yield and thermal performance of an inclined SS. A ANFIS model was utilized to predict the water yield of a double-slope SS with a hemispherical basin under Egyptian conditions [36]. A hybrid ANN model was developed to predict the water yield of an active SS [34]. The performance of a stepped SS with a corrugated absorber plate was predicted using a long-short memory ANN model [27].

In all above mentioned studies ML approaches have been reported as accurate and reliable tools to predict the water yield of SSs' types. ML models can be trained using a few experimental data. After the training process, ML models can be used to predict the water yield for conditions that it has not seen before. Using ML approaches helps in avoiding carrying out more costly experiments or solving complicated mathematical models.

Therefore, there are two main contributions of this study. The first contribution is developing a low-cost efficient bilayered structure that used in a SS to efficiently convert the absorbed solar energy into heat which localized on thin water film rather than bulk water. This bilayered structure is composed of an AL (black cotton fabric) wrapping onto a SL (polystyrene foam). The developed bilayered structure is floated on water surface inside a SS tested under real world conditions. The performance of the MSS (with HLBS) is compared with a CSS (without HLBS) considering three process responses, namely freshwater productivity, energy efficiency, and exergy efficiency. Cost analysis is performed of the proposed bilayered structure compared with other improving techniques used to augment SS performance. The second contribution is applying three different ML approaches to predict the water yield of both SSs. The ML approaches are ANN, ANFIS, and SVM. The quality of the ML approaches is evaluated using seven different statistical measures. The rest of this paper introduces the following:

- The experimental setup and measuring instruments is presented.
- The proposed material structure is introduced.
- The theoretical background is explained including: thermal analysis, uncertainty analysis, cost analysis, and the machine learning approaches.
- The obtained results are discussed.
- The main conclusions are presented.

Table 2
Specifications of measuring instruments

Measured parameter	Instrument	Accuracy	Operating range	Error (%)
Temperature	K-type thermocouples	±0.1 °C	−100–500 °C	0.75
Solar irradiance	Solar power meter	±5 W/m^2	0–2000 W/m^2	2
Productivity	Graduated cylinder	±2 ml	0–1000 ml	1

Experimentation

In this study, two similar SSs were manufactured; the first one is a MSS in which an HLBS is embedded while the second is a CSS as shown in Fig. 1. The CSS was used as a reference to assess the productivity and the thermal performance of the first SS. Both SSs have the same geometrical dimensions (0.4 m length, 0.4 m width, 0.08 m front height, and 0.32 m back height) and the angle between the glazier cover and the basin (the horizontal) was set at 31° which equals to the longitude of the place of experiments[91]. So, the area of the basin for each SS is 0.16 m^2. The basin of the SS is made of a galvanized steel sheet with a thickness of 1 mm and covered by a glazier cover with 3 mm thickness. The inner basin's surfaces were coated by a black paint with high absorptivity to enhance the harvesting of solar energy while all external surfaces were insulated by fiber glazier with 15 mm thickness which acts as a thermal barrier to lessen heat losses to the surroundings. The interface between the galas cover and the basin was sealed by silicon to inhibit any vapor leakage. The experiments were performed within daytime from 6 AM to 6 PM. The measured parameters were solar radiation intensity, ambient temperature, the water and glazier temperatures, HLBS surface temperature, and the amount of water yield. All these parameters were measured at hourly intervals. The brackish water is supplied to the SSs by a pipe system connected to a water tank and the flow is controlled using feed valves. Six K-type thermocouples (K 7/32-2C-TEF) were utilized to measure the temperature of ambient, glazier cover, water, and HLBS surface. Temperature indicator (DTC324A-2) was used to record the measured temperatures. The solar irradiance was measured using TM-207 solar meter. A graduated cylinder was used to measure the distillate output. The accuracy and the operating range of the used instruments are tabulated in the Table 2.

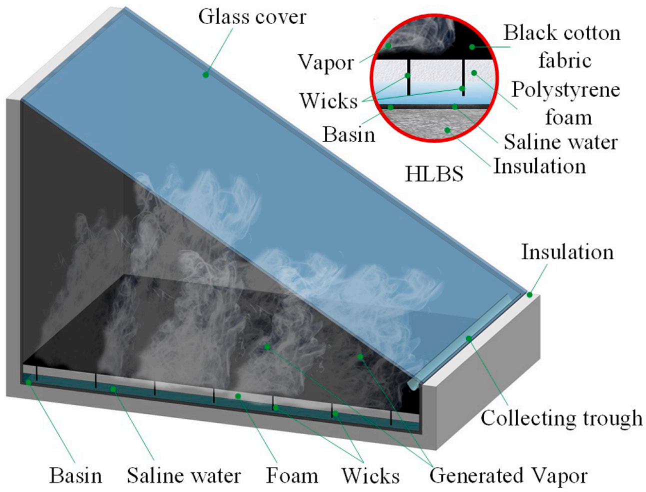

Fig. 2. Modified solar still with HLBS.

Material structure

The proposed heat localization structure consists of a black cotton fabric wrapped over a polystyrene foam sheet (2 cm thick) as shown in Fig. 2. This hybrid material structure is inspired by bifunctional cotton fabric developed by Hao et al. [44]. The black cotton fabric has a high sunlight absorptance and acts as an AL, while the polystyrene foam acts as a thermal insulator and acts as SL for the absorber that floats on water surface due to its low density (0.05 g/cm^3). The foam sheet has many holes in which hydrophilic cotton wicks are inserted to transfer water from water bulk to the black cotton fabric via capillary action. When the solar radiation strikes the HLBS it is trapped and absorbed by the cotton fabric layer and converted into thermal energy which confined in the cotton fabric layer. This confined heat is utilized to heat a thin layer of water instead of bulk basin water. Heated up water begins to evaporate and it condenses when it strikes the inner surface of the glazier cover. Then, the condensed water is collected using a collecting trough for further tests.

Theoretical background

In this section the basis of four main topics will be discussed, namely, thermal analysis, uncertainty analysis, cost analysis and machine learning approaches.

Thermal analysis

Heat transfer process in this arrangement has three main modes: evaporation, convection and radiation. These modes of heat transfer take place inside the SS enclosure. The external heat transfer occurs mainly between the outer glazier cover surface and the ambient air via two main modes: convection and radiation. While the heat transferred from basin to the ambient is neglected due to thermal insulation.

The hourly energy efficiency, η_{eh}, is is given by:

$$\eta_{eh} = \frac{\dot{m}_w \times L}{I(t) \times A_b \times 3600} \tag{1}$$

where $\dot{m}_w$, L, $I(t)$, and A_b denote distillate output (kg/m^2.h), the latent heat of evaporation (J/kg), solar radiation(W/m^2), and basin area (m^2), respectively.

Where; the latent heat of evaporation L could be calculated as a function in water temperature T_w using the following formula [14]:

$$L = 2501.9 \times 10^3 - 2.40406 \times 10^3 T_w + 1.19221 {T_w}^2 - 1.5863 \times 10^{-2} {T_w}^3 \tag{2}$$

The hourly exergy efficiency, η_{xh}, is given by[99]:

$$\eta_{xh} = \frac{\dot{E}_{ev}}{\dot{E}_{ir}} \tag{3}$$

where $\dot{E}_{ev}$ and $\dot{E}_{ir}$ denote exergy of evaporation (J) and exergy of solar irradiance (J), respectively; and they are given by:

$$\dot{E}_{ev} = I(t) \times A_b \times P \tag{4}$$

$$\dot{E}_{ir} = \frac{\dot{m}_w \times L}{3600} \times \left(1 - \frac{T_a}{T_w}\right) \tag{5}$$

where T_a and T_w are ambient and water temperatures (K), respectively; and P is Petela expression given by [78]:

$$P = 1 + \frac{1}{3}\left(\frac{T_a}{T_s}\right)^4 - \frac{4}{3}\left(\frac{T_a}{T_s}\right) \tag{6}$$

where T_s is sun temperature (6000 K).

Uncertainty analysis

The uncertainty analysis is performed based on the mathematical approach proposed by[46]. Assuming that a set of measurement is carried out to measure n process input variables which used to calculate some responses (R). Thus:

$$R = (X_1, X_2, X_3 \cdots, X_n) \tag{7}$$

The uncertainty in response U_R can be calculated in terms of the uncertainties in the independent variables U_1, U_2, U_3,………U_n as follows:

$$U_R = \left[\left(\frac{\partial R}{\partial X_1} U_1\right)^2 + \left(\frac{\partial R}{\partial X_2} U_2\right)^2 + \cdots + \left(\frac{\partial R}{\partial X_n} U_n\right)^2\right]^{\frac{1}{2}} \tag{8}$$

The measurement uncertainties (error) of different experimental instruments including K-type thermocouples, solar power meter, and graduated cylinder are listed in Table 2.

The minimum error is calculated as the ratio between the least count of errors and the minimum measured value of the output, while the least count error is defined as the error related to the instrument resolution [5].

The measured distillate output $\dot{m}_w$ value is a function of the water height (h_w) in the graduated cylinder. Following Eq. (7), the uncertainty of the hourly measured distillate output can be calculated by:

$$U_{m_w} = \left[\left(\frac{\partial m_w}{\partial h_w} U_{h_w}\right)^2\right]^{\frac{1}{2}} \tag{9}$$

The hourly energy efficiency, η_{eh}, is function of the hourly measured distillate output $\dot{m}_w$, the latent heat of vaporization L, and solar irradiance $I(t)$. And L is a function of the water temperature T_w.

Then the total uncertainty of the energy efficiency can be calculated by:

$$U_{\eta_{eh}} = \left[\left(\frac{\partial \eta_{eh}}{\partial m_w} U_{m_w}\right)^2 + \left(\frac{\partial \eta_{eh}}{\partial I} U_I\right)^2 + \left(\frac{\partial \eta_{eh}}{\partial T_w} U_{T_w}\right)^2\right]^{\frac{1}{2}} \tag{10}$$

On the other hand, the hourly exergy efficiency, η_{xh}, is function of the hourly measured distillate output $\dot{m}_w$, the latent heat of vaporization L, ambient temperature T_a, and solar irradiance $I(t)$. And L is a function in the water temperature T_w.

$$U_{\eta_{xh}} = \left[\left(\frac{\partial \eta_{xh}}{\partial m_w} U_{m_w}\right)^2 + \left(\frac{\partial \eta_{xh}}{\partial I} U_I\right)^2 + \left(\frac{\partial \eta_{xh}}{\partial T_w} U_{T_w}\right)^2 + \left(\frac{\partial \eta_{xh}}{\partial T_a} U_{T_a}\right)^2\right]^{\frac{1}{2}} \tag{11}$$

The calculations are performed based on the aforementioned formulas showed that the uncertainty in the measured productivity, energy efficiency and exergy efficiency are ±0.5%, ±1%, and ±1.5%, respectively.

Cost analysis

The main advantages of SS based desalination technology over other desalination technologies is its low cost and simplicity. The developed low cost HLBS is made from low cost materials: polystyrene foam and black cotton fabric; which gives it a more advantages over other integrated techniques with SSs such as solar collectors, vacuum fans, and nanofluids. In this subsection the economic analysis of the MSS is introduced. The cost analysis could be conducted via applying the following procedures considering different parameters affecting the SS productivity[19,101]:

$$SFF = \frac{i}{(i+1)^n - 1} \tag{12}$$

where *SFF*, *n*, *i*, denote the sinking fund factor, the number of operating years (assumed to be 10 years), the interest per year (assumed to be 12%/year), respectively.

$$CRF = SFF \times (i+1)^n \tag{13}$$

CRF denotes the capital recovery factor.

$$FAC = P \times CRF \tag{14}$$

FAC and *P* denote the fixed annual cost ($) and the present capital cost ($), respectively. Then, the salvage value *S* ($) and the annual salvage value *ASV* ($) are calculated as follows:

$$S = 0.2 \times P \tag{15}$$

$$ASV = SFF \times S \tag{16}$$

The annual maintenance operational cost *AMC* ($) is calculated as follows [102]:

$$AMC = 0.15 \times FAC \tag{17}$$

Then, the annual cost *AC* ($) is given by:

$$AC = AMC + FAC - ASV \tag{18}$$

Finally, the cost of distilled water per liter *CPL* ($/l) is given by:

$$CPL = \frac{AC}{M} \tag{19}$$

where *M* denotes annual yield (l).

Machine learning approaches

ML is a smart type of artificial intelligence that has advanced learning capabilities which enables it to model different engineering systems. In this study, three ML methods are applied to predict the water yield of the examined solar still. The theoretical background of ANN and ANFIS could be found in our previous published articles [7,21,26,28]. Herein, the basis of SVM is introduced.

SVM is a ML method that used to model the relationship between a process response and process descriptors. The response of SVM can have different form such as normal, Poisson, binomial. These forms give SVM advantages over simple linear regression or exponential regression which have responses with a normal distribution form. In a typical SVM model, a link function L is used to describe the linear relationship. SVM applies a regularization technique to reduce the model complexity by applying a penalty term. This regularization technique also helps in identifying the dominant descriptors and reducing the number of coefficients. The training data has been chosen randomly despite of the negligible effect of randomization on the model's prediction accuracy [48].

In the SVM regression, a training set *x* is introduced to the model and it is mapped to a feature space with *n* dimensions. The link function that used to construct the model in the feature space is given by:

$$L(x, \varepsilon) = \sum_{i=1}^{n} \varepsilon f_i(x) + c \tag{20}$$

Here, $\mu_i(y)$ $f_i(x)$ denotes multiple nonlinear transformations,ω_i ε denotes the weights of the model, and s c is the applied bias.

The predicting ability of the SVM model can be evaluated via computing a loss function. The kernel function Γ of the SVM regression model is given by:

$$\Gamma(x, x_j) = \sum_{i=1}^{n} f_i(x) f_i(x_j) \tag{21}$$

The accuracy and the generalization capability of SVM are highly dependent on the used kernel parameters. There are many types of kernel functions that can be embedded in SVM such as Laplace, Gaussian, and spline. Among all these kernel functions Gaussian kernel k has been reported as an efficient kernel function that outperforms the other. Gaussian kernel function is given by:

$$\Gamma_G(x, y) = exp\left(-\frac{\|x-y\|^2}{2\sigma^2}\right) \tag{22}$$

There many error metrics that adopted to adjust the parameters of SVM models. One of the common used error functions is given by:

$$y_i = \sum_{i \neq 1} y_i \Gamma(x_j, x_i) \tag{23}$$

This error function is used as an objective function which should be minimized to obtain the optimal model parameters that maximize the model accuracy.

Evaluation criteria

Statistical measures are used to evaluate the performance of ML models. The most common used statistical metrics are root mean square error (RMSE), coefficient of determination (R^2), mean absolute error (MAE), mean relative error (MRE), overall index (OI), efficiency coefficient (EC), and coefficient of variation (COV) [23,25].

RMSE can be calculated as:

$$RMSE = \sqrt{\frac{1}{g} \sum_{i=1}^{g} (d_i - y_i)^2} \tag{24}$$

R^2 is calculated by:

$$R^2 = \frac{\left(\sum_{i=1}^{g} \left(d_i - \overline{d}\right)(y_i - \overline{y})\right)^2}{\sum_{i=1}^{g} \left(d_i - \overline{d}\right)^2 \times \sum_{i=1}^{g} (y_i - \overline{y})^2} \tag{25}$$

MAE and MRE are used to assess the model accuracy. The low values of MAE and MRE indicate the high accuracy of the model. They are calculated by[24]:

$$MRE = \frac{1}{n_s} \sum_{i=1}^{g} \frac{d_i - y_i}{d_i} \tag{26}$$

$$MAE = \frac{1}{n_s} \sum_{i=1}^{g} |d_i - y_i| \tag{27}$$

EC predicts the model accuracy and has numerical values range between $-\infty$ and 1. It can be calculated by [58]:

$$EC = 1 - \frac{\sum_{i=1}^{g} (d_i - y_i)^2}{\sum_{i=1}^{g} \left(d_i - \overline{d}\right)^2} \tag{28}$$

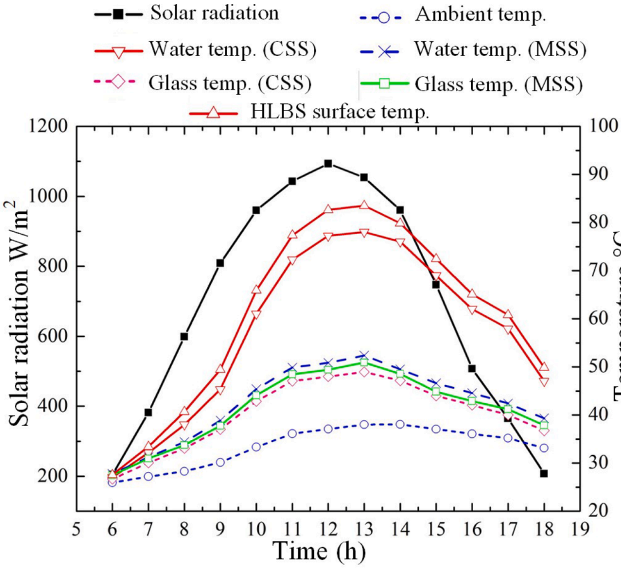

Fig. 3. Variation of solar irradiance, air temperature, glazier temperature, water temperature, and HLBS surface temperature with respect to time.

OI and COV are computed as functions of the RMSE and EC. Optimal model accuracy can be obtained if the COV value approaches zero and the OI value approaches the unity. They are given as[33]:

$$OI = \frac{1}{2}\left(1 - \left(\frac{RMSE}{d_{max} - d_{min}}\right) + EC\right) \tag{29}$$

$$COV = \left(\left(\frac{RMSE}{\overline{y}}\right) \times 100\right) \tag{30}$$

where *m*, *x, and d* denote the number of datasets, experimental and the predicted values respectively. d_{max} is the maximum value of experimental data, d_{min}dmindmax is the minimum value of experimental data and $\overline{d}$d is the mean value of experimental data, while ȳ $\overline{y}$ denotes the mean value of the predicted data.

Results and discussion

The main topics discussed in this section are:

- The effect of the use of HLBS on the water yield and thermal performance of SS.
- The cost analysis of the proposed MSS.
- The prediction of water yield using ML approaches.

Before analyzing the thermal performance of the developed SSs, the measured operating parameters will be introduced. The measured values of solar irradiance, ambient temperature, glazier temperature, water temperature and HLBS surface temperature were recorded during the daytime (6 AM-6 PM). All measured temperatures as well as solar irradiance considering a constant water depth of 1 cm are plotted in Fig. 3. The solar irradiance and ambient temperature are the main independent variables that affect the performance of SSs. While other measured parameters: water temperature, glazier temperature, and HLBS surface temperature are dependent on the aforementioned independent variables as well as the SS design and geometry. Monitoring both of independent and dependent parameters during the operation of SS plays a key role in assessing the thermal performance of the SS and in understanding the effect of different parameters and design modifications on the SS performance.

At the beginning of the experiment (6 AM), the solar irradiance has a low value of 204 W/m^2, which increases till reaching a peak value of

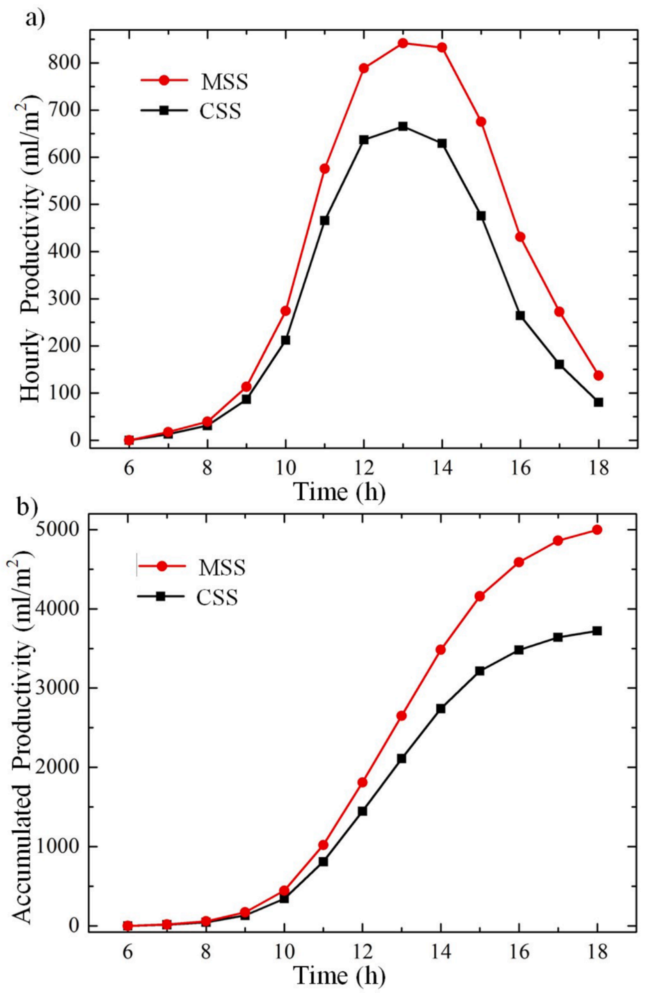

Fig. 4. a) Hourly water yield of SS with and without HLBS; b) Accumulated water yield of SS with and without HLBS.

1093 W/m^2 at 12 PM, and then smoothly decreases to 207 W/m^2 at 6 PM. For the ambient temperature, it has a low value of 25.94 °C at the start of the experiment, which increases till reaching a peak value of 38.07 °C at 2 PM, and then smoothly decreases to 33.14 °C at 6 PM. For the CSS, both of glazier and water temperatures reach their peak values of 48.96 °C and 78.05 °C, respectively, at 1 PM. For the MSS, both of glazier and water temperatures reach their peak values of 50.92 °C and 52.39 °C, respectively, at 1 PM; while the temperature of HLBS surface has a peak value of 83.51 °C at 1 PM. There is a notable decrease in CSS water temperature (about 26 °C) compared with that of MSS. That is due to that the received solar energy is exploited in heating up a thin layer of water in case of MSS instead of water bulk in case of CSS. Moreover, there is a reasonable increase in HLBS surface temperature (about 5 °C) compared with water temperature of CSS which gives an advantage to MSS over CSS as it results in increasing the evaporation rate and the productivity of MSS compared with CSS. The higher temperature difference between the water surface and the glazier cover of MSS (about 35.59 °C) compared with that of CSS (about 29.09 °C) may enhance the circulation process of humid air inside the SS and the condensation of vapor on the inner surface of the glazier cover.

The hourly productivity of both SSs (with and without HLBS) is plotted in Fig. 4. At the start of the experiment, the yield of both SSs is equal to zero. Then, the MSS yield exceeds the CSS yield by 4.2 ml at 7 AM. The difference between the yields of both SSs increases with time till it reaches a peak value of 203.2 ml at 1 PM and then it declines during the daytime until sunset and reaches a value of 56.6 ml at 6 PM.

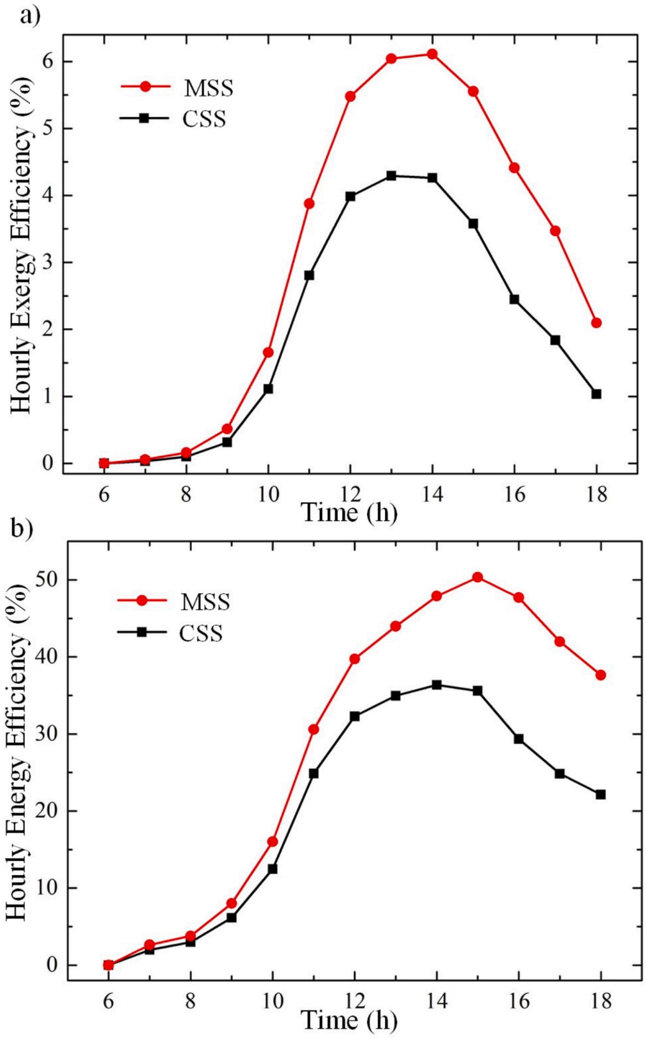

Fig. 5. a) Hourly exergy efficiency of SS with and without HLBS; b) Hourly energy efficiency of SS with and without HLBS.

At the end of the experiment, the hourly productivity of CSS and MSS was 80.2 ml and 136.8 ml, respectively. The accumulated productivity of both stills is plotted in Fig. 4, it was 3.70 L/day and 4.99 L/day for the CSS and MSS, respectively, with an increase of 34.32% in the water yield during the day.

The hourly energy and exergy efficiencies of both SSs (with and without HLBS) are plotted in Fig. 5. For CSS, the hourly exergy efficiency increases from the beginning of the experiments with time till reaching its peak value (4.29%) at 1 PM and it approximately maintains this peak value for another more hour (2 PM), then it declines with time and has a low value of 1.03% at 6 PM. For MSS, the hourly exergy efficiency also increases from the beginning of the experiments with time till reaching its peak value (6.10%) at 2 PM, then it declines with time and has a low value of 2.09% at 6 PM. The difference between the exergy efficiency of MSS and CSS increased at the end of the day as shown in Fig. 5 (a). The improvement in exergy efficiency for MSS over CSS has its peak value (about 102%) at 6 PM; however, it has a low value of (approximately 40%) at the noon. That indicates the effectiveness of the developed HLBS to exploit the solar energy to evaporate water even at the sunset time at which the solar radiation has low values. The same trend is observed for the energy efficiency as shown in Fig. 5 (b). The hourly energy efficiency of MSS is higher than that of CSS for all investigated hours. For CSS, the energy efficiency reaches its peak value (36.35%) at 2 PM and declines with time till reaching its minimal value (22.12%) at 6 PM. For MSS, the

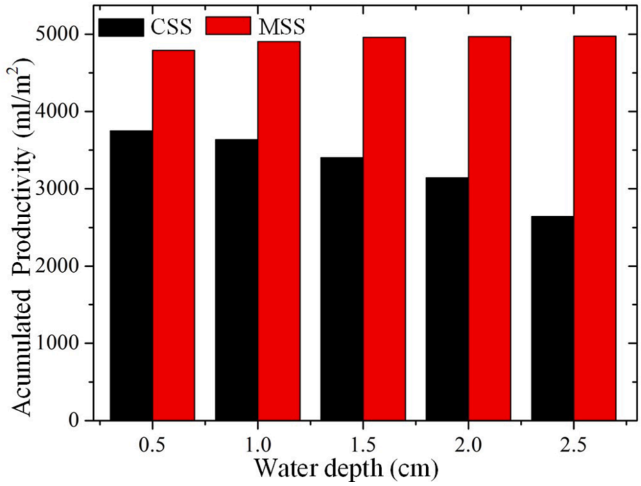

Fig. 6. The effect of the water thickness on accumulated water yield of CSS and MSS.

Table 3
Cost data of different components of MSS.

Component	Cost ($)
Basin	40
Glazier cover	10
Water tank	5
Pipes and valves	10
Silicon and paints	10
Insulation	10
Polystyrene foam sheet (for MSS only)	2
Black cotton fabric (for MSS only)	8
Manufacturing	25

energy efficiency reaches its peak value (50.34%) at 3 PM and declines with time till sunset and has a reasonable value (37.64%) at 6 PM. The improvement in the energy efficiency for the MSS over CSS has a peak value (70.11 %) at 6 PM; however, it has a low value of (approximately 25%) at the noon. Moreover, the daily overall energy efficiency of CSS and MSS is 23.24% and 31.09%, respectively. The daily overall exergy efficiency of CSS and MSS is 2.47% and 3.63%, respectively. These results revealed the superior thermal performance of MSS compared with CSS and the effectiveness of using HLBS in SS to augment the water evaporation and fresh water productivity.

To figure out the effect of water depth in the basin on the freshwater productivity of SSs, another set of experiments was conducted. For the CSS, the water depth affects the fresh water productivity as reported by [54] and plotted in Fig. 6. As shown in that figure the freshwater productivity deceases with increasing the water depth. The accumulated productivity of CSS is decreased by about 1100 ml (40%) when the water thickness increased from 0.5 cm to 2.5 cm. For MSS, increasing the water depth has a positive effect on productivity unlike CSS. The accumulated productivity of MSS is increased by about 250 ml (5%) when the water thickness increased from 0.5 cm to 2.5 cm. Therefore, change of water depth has a considerable effect on the freshwater productivity of CSS compared with that of MSS. That is due to the heat localization process which occurs in MSS which lessens the energy consumed in heating the bulk water in the basin and concentrates the heating process on the water surface where the evaporation occurs.

The cost data according to the Egyptian local market of the different MSS components are listed in Table 3. Assuming the maintenance process requires one day per week (52 day per year), and then the operating period for the cost analysis is 310 days per year. The maintenance process includes several steps such as brackish water filling, glazier cover cleaning, corners and edges sealing, removing brine water, and

Table 4
Cost analysis for the developed MSS.

P($)	SFF	CRF	FAC ($)	S ($)	ASV ($)	AMC ($)	AC ($)	M (l)	CPL ($/l)
120	0.057	0.177	21.15	24.1	1.35	3.15	23.25	1550	0.015

Table 5
A comparison between different SS investigations found in literature.

Ref.	AC ($)	M (l)	CPL ($/l)
This study	23.25	1550	0.015
[81]	18.06	681	0.0265
[15]	21.13	559	0.0378
[104]	30.74	429	0.0717
[97]	50.34	1196	0.0421
Fath et al. [39]	19.12	1170	0.0163

Table 6
Cost of SS improving techniques found in literature [10,20,51,115].

Improving technique	Cost ($/m^2)	Productivity improvement (%)
Solar concentrator	50–100	18
Nanofluids	10–20	12–30
Sun-tracking system	50–100	22–30
Nano-coating of condensing surface	10–20	20–50
Shallow solar pond	70–150	43–55
Solar collector	140–800	36–250
HLBS (this study)	10–15	34 %

distilled water collecting. The different values of *SFF*, *CRF*, *S*, *ASV*, *FAC*, *AC*, *AMC*, and *CPL* are listed in Table 4. The developed MSS has a reasonable cost of freshwater per liter (0.015 $/l) and annual yield compared with other studies found in literature as tabulated in Table 5. The developed HLBS is characterized as an efficient low cost steam generation device as it enhances the fresh water productivity by about 34% using low cost materials (10 $/m^2) compared with other improvement techniques found in literature as tabulated in Table 6.

The water yield of the established SSs was predicted using three different ML approaches, namely, ANN, ANFIS, and SVM. All ML models were trained using experimental data collected during seven days. The total number of the datasets are 84, 80% of them were used to train the models and the 20% of them were used to test the models. The model inputs are solar irradiance and ambient temperature, while the model output was the water yield. The experimental data used in training the ML models are plotted in Fig. 7. Fig. 8 shows the correlation matrix between the inputs and outputs of the models. The statistical analysis based on minimum, maximum, average and standard deviation of the experimental data is tabulated in Table 7. These data is normalized based on its mean and variance before it be used as training data sets of the proposed models.

The predicted water yield using SVM showed better consistency with the experimental one, in contrary to that of ANN and ANFIS which deviated from the experimental data as observed in Fig. 8.

Fig. 9 (a-c) displays that the QQ-plots of the experimental and the predicted values of water yield using ANN, ANFIS and SVM, respectively. The plotted points is scattered randomly around the straight line in case of ANN and ANFIS models. In case of SVM, the plotted points lie on or in vicinity of the straight line. Therefore, it can be declared that: the best regression fit between the predicted and target water yield is obtained using SVM, followed by ANFIS, and lastly, the worst regression fit between the predicted and target is obtained by ANN. Furthermore, the normalized error histograms for the three models are demonstrated in Fig. 9 (d-f) for ANN, ANFIS, and SVM, respectively. The highest normalized error was attained by ANN algorithm followed by ANFIS, and lastly, SVM has the smallest value of the normalized errors. Furthermore, it can be observed from the normalized error histograms that the error attained by ANN and ANFIS follows a normal distribution with high normalized errors, while the error obtained by SVM does not follow a normal distribution with small normalized error. The same trend is observed in case of MSS for QQ-plots as shown in Fig. 10 (a-c) and normalized error histograms as shown in Fig. 10 (d-f). Therefore, the SVM model can be declared as an accurate model compared with the other two models to predict the water yield for both of CSS and MSS.

The performance of the proposed SVM was compared with the other two models (ANN and ANFIS) using seven statistical measures, namely, RMSE, R^2, MAE, MRE, EC, OI, and COV. The evaluation of the three ML models using different statistical measures is presented in Fig. 11 and

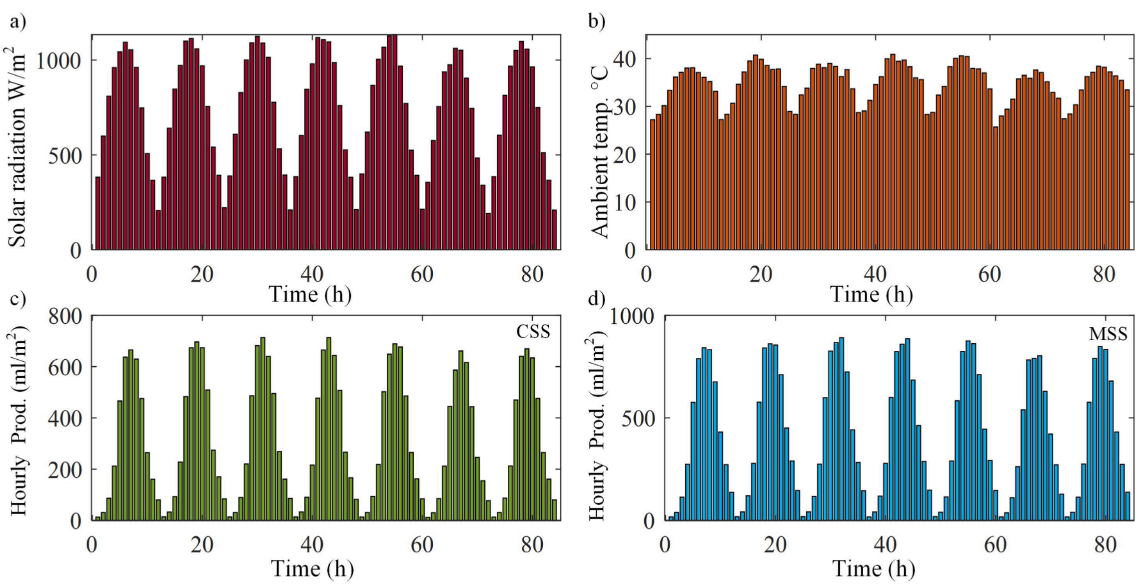

Fig. 7. The measured experimental data: a) solar radiation; b) ambient temperature, c) the hourly water yield of CSS; d) the hourly water yield of the CSS.

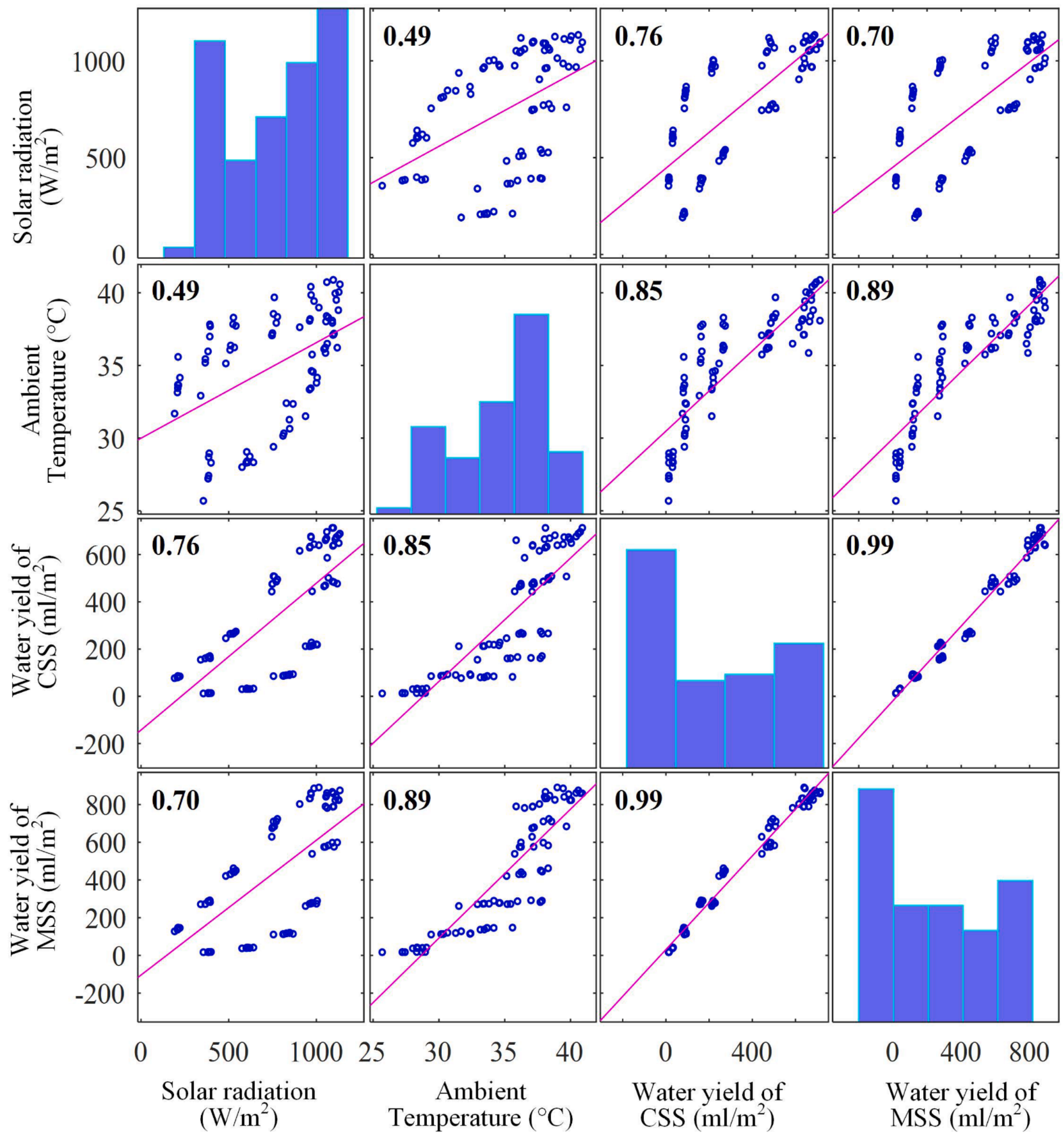

Fig. 8. The correlation matrix between the input and output variables.

Table 7
Statistical analysis of the experimental data.

	Solar radiation	Ambient temperature	Water yield of conventional SS	Water yield of modified SS
Maximum	1133.722	40.889	713.253	890.998
Minimum	191.205	25.686	12.099	17.207
Average	738.467	34.853	316.606	424.187
Standard Deviation	301.891	4.022	247.531	310.072

Table 8. SVM outperforms the other two models in predicting the water yield for both SSs in terms of all statistical measures as depicted in spider plots presented in Fig. 12. For both SSs, SVM has the highest values of R^2, OI, and EC followed by ANFIS and ANN models. Besides, SVM has the lowest values of RMSE, MAE, MRE, and COV followed by ANFIS and ANN models. The high values of R^2, OI, and EC as well as the low values of RMSE, MAE, MRE, and COV indicate the high accuracy of the SVM over the other two models. From Table 8, the values of R^2, OI, and EC of SVM approaches the unity as all of them has a very close value to the unity (0.999) for both SSs; the approaching of these values to the unity indicate the ultimate accuracy of SVM. Moreover, the values of RMSE, MAE, MRE, and COV tends to vanish as all of them has a very close value to zero which are 0.099, −0.001, 0.098, and 0.031 for CSS and 0.098, −0.001, 0.098, and 0.023 for MSS, respectively; the approaching of these values to zero indicate the ultimate accuracy of SVM. These results reveal the outperformance of SVM model over ANN and ANFIS for predicting the water for both SSs.

Conclusions

In this study, a new heat localization bilayered structure is proposed to improve the performance of solar stills (SSs). The thermal performance and the cost of the developed SS was analyzed. Moreover, the water yield of the developed SSs was predicted using three machine learning approaches, namely, ANN, ANFIS, and SVM. The bilayered structure consists of an AL made of black cotton fabric wrapped on a SL made of polystyrene foam. The AL absorbs solar energy with high efficiency, while the low density foam enables the bilayered structure to float on the surface of saline water and its low thermal conductivity confine heat in the AL via insulating the AL from the water bulk. Using the developed structure, the rate of evaporation is increased and the heat losses are decreased, which enhance the productivity and the thermal

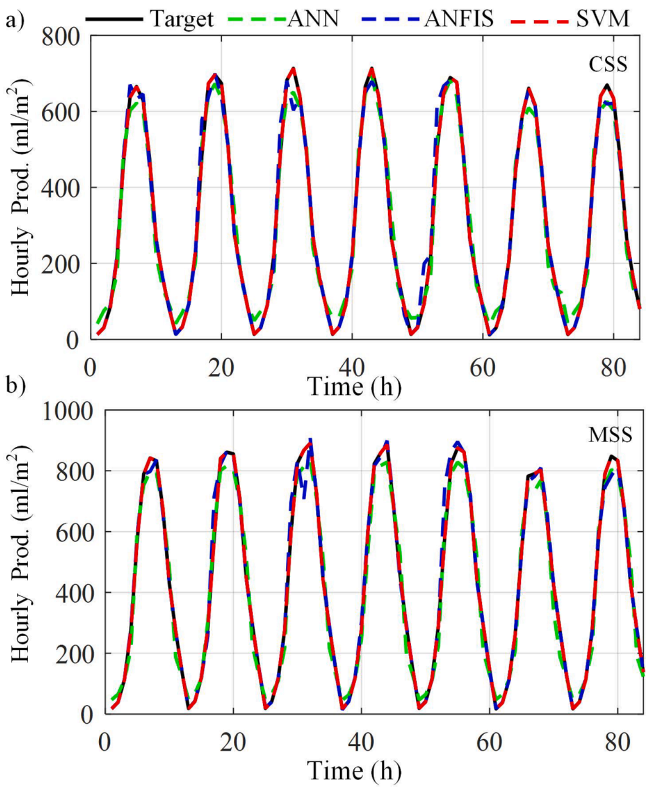

Fig. 9. The predicted water yield using different ML approaches: a) CSS; b) MSS.

performance of the SS. The effects of the developed bilayered structure and the water depth in the basin on the SS performance have been investigated. The water yield of the MSS is always greater than that of the reference still for all water depths. The obtained results revealed the superior thermal performance of MSS compared with CSS and the effectiveness of using HLBS in SS to augment the water evaporation and fresh water yield. The following conclusions could be drawn from the current study:

- The maximum water yield achieved in case of MSS is 4.99 L/m2/day which is higher than that of CSS by about 34%.
- The daily overall energy efficiency of CSS and MSS is 23.24% and 31.09%, respectively.
- The daily overall exergy efficiency of CSS and MSS is 2.47% and 3.63%, respectively.
- The water depth in the basin does not significantly affect the water yield of MSS.
- The water yield of CSS decreased by about 1100 ml (40%) when the water thickness increased from 0.5 cm to 2.5 cm.
- The water yield of MSS increased by about 250 ml (5%) when the water thickness increased from 0.5 cm to 2.5 cm.
- The cost of freshwater per liter obtained by the modified solar still is 0.015 \$/l which is reasonable compared with other improving techniques used in literature.
- SVM outperformed ANN and ANFIS in predicting the water yield of both SSs.
- A high coefficient of correlation of 0.999 was obtained using SVM.

For future work, it is recommended to apply advanced artificial intelligence models such random vector functional link to model the water yield and thermal performance of solar stills. Moreover, advanced metaheuristic optimizers could be used to optimize the performance of the model as well as desalination system. The quality of the produced

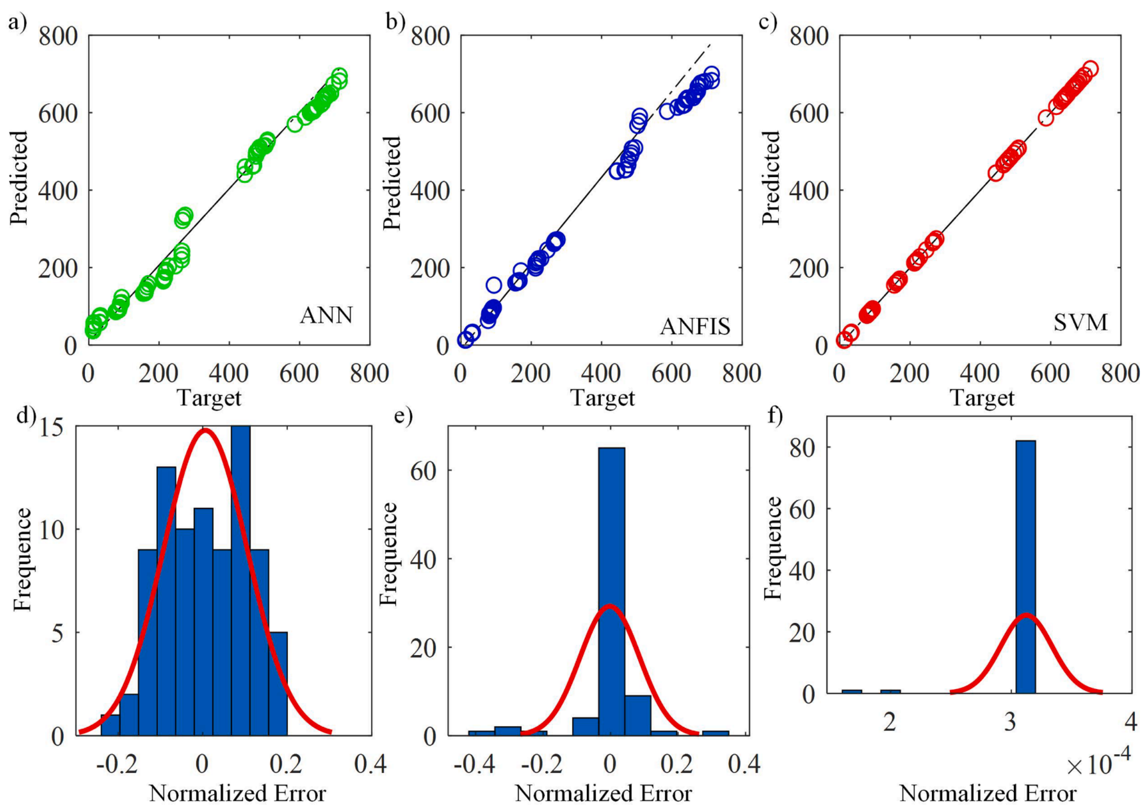

Fig. 10. The qq-plot of target (experimental) and the predicted water yield of CSS (a) ANN, (b) ANFIS, (c) SVM and the normalized error histogram for (d) ANN, (e) ANFIS (f) SVM.

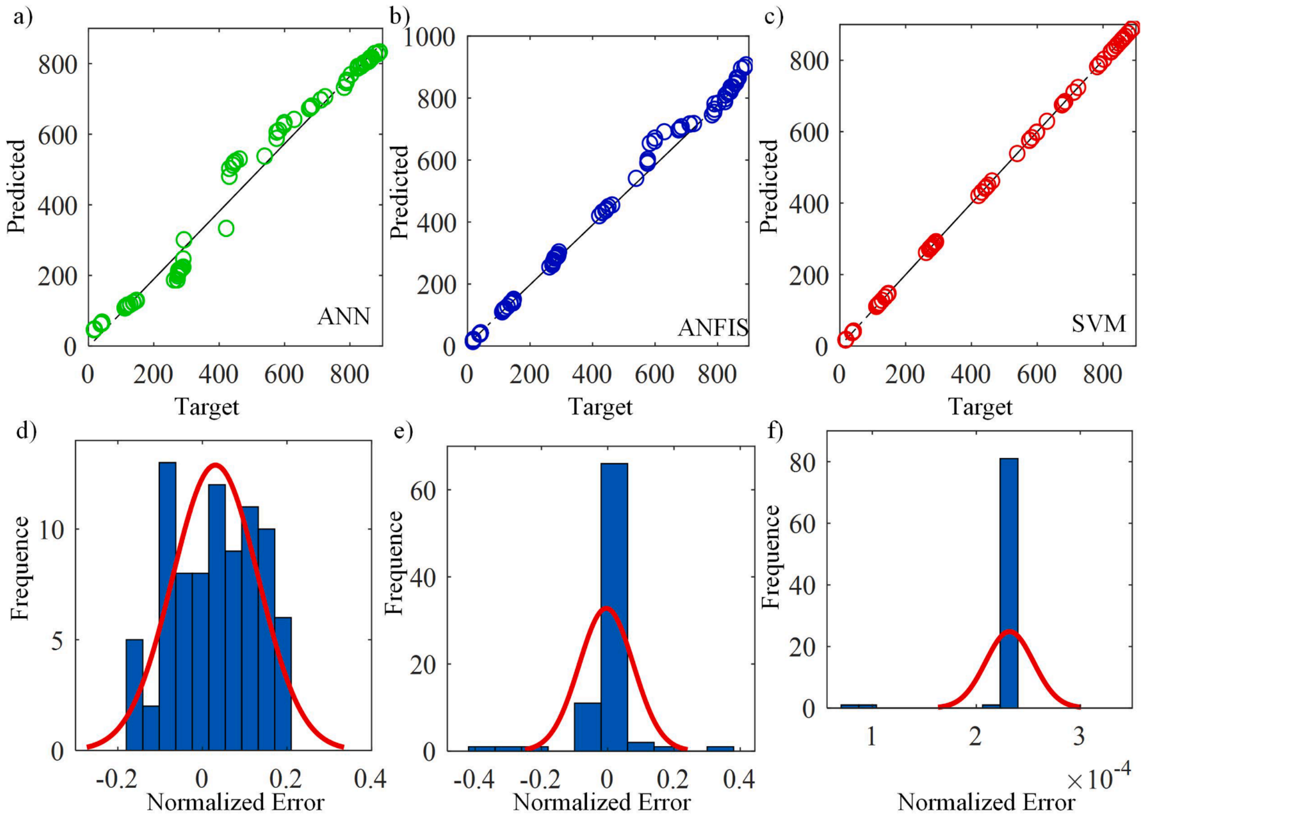

Fig. 11. The qq-plot of target (experimental) and the predicted water yield of MSS (a) ANN, (b) ANFIS, (c) SVM and the normalized error histogram for (d) ANN, (e) ANFIS (f) SVM.

Table 8
Statistical measures used to evalute the performance of the three ML models.

		R^2	RMSE	MRE	MAE	COV	EC	OI
CSS	ANN	0.986	31.445	0.301	27.351	9.994	0.983	0.969
	ANFIS	0.987	27.773	0.013	12.798	8.751	0.987	0.973
	SVM	0.999	0.099	−0.001	0.098	0.031	0.999	0.999
MSS	ANN	0.981	44.699	0.137	37.999	10.872	0.978	0.963
	ANFIS	0.987	34.514	0.005	14.654	8.101	0.987	0.973
	SVM	0.999	0.098	−0.001	0.098	0.023	0.999	0.999

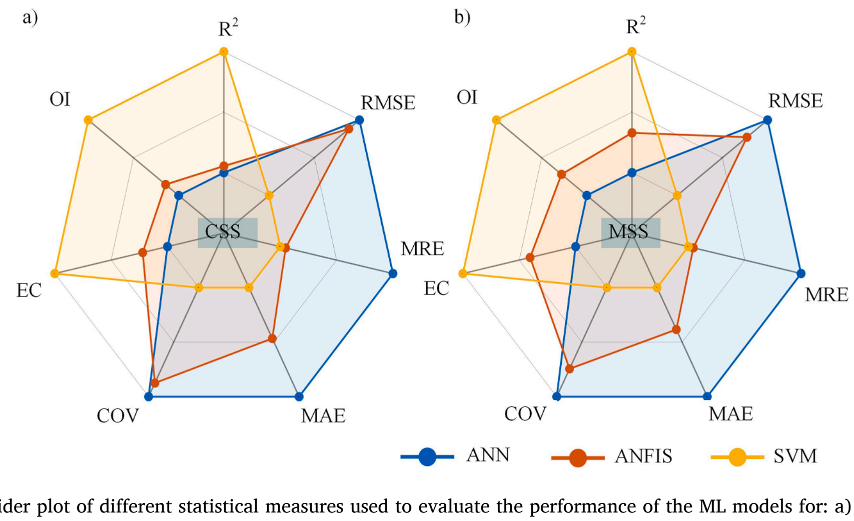

Fig. 12. Spider plot of different statistical measures used to evaluate the performance of the ML models for: a) CSS; b) MSS.

water and the sustainability of the desalination system are also good research directions that should be extensively investigated.

Declaration of Competing Interest

The authors declare that they have no known competing financial interests or personal relationships that could have appeared to influence the work reported in this paper.

Reference

[1] Abd Elaziz M, Essa FA, Elsheikh AH. Utilization of ensemble random vector functional link network for freshwater prediction of active solar stills with nanoparticles. Sustainable Energy Technol Assess 2021;47:101405. https://doi.org/10.1016/j.seta.2021.101405.
[2] Abdeen A, Serageldin AA, Ibrahim MGE, El-Zafarany A, Ookawara S, Murata R. Solar chimney optimization for enhancing thermal comfort in Egypt: an experimental and numerical study. Sol Energy 2019;180:524–36.
[3] Abdessemed A, Bougriou C, Guerraiche D, Abachi R. Effects of tray shape of a multi-stage solar still coupled to a parabolic concentrating solar collector in Algeria. Renewable Energy 2019;132:1134–40.
[4] Aghaei Zoori H, Farshchi Tabrizi F, Sarhaddi F, Heshmatnezhad F. Comparison between energy and exergy efficiencies in a weir type cascade solar still. Desalination 2013;325:113–21.
[5] Agrawal A, Rana RS, Srivastava PK. Heat transfer coefficients and productivity of a single slope single basin solar still in Indian climatic condition: experimental and theoretical comparison. Resour-Effic Technol 2017;3(4):466–82.
[6] Appadurai M, Velmurugan V. Performance analysis of fin type solar still integrated with fin type mini solar pond. Sustainable Energy Technol Assess 2015;9:30–6.
[7] Babikir HA, Elaziz MA, Elsheikh AH, Showaib EA, Elhadary M, Wu D, et al. Noise prediction of axial piston pump based on different valve materials using a modified artificial neural network model. Alexandria Eng J 2019;58(3):1077–87.
[8] Bae K, Kang G, Cho SK, Park W, Kim K, Padilla WJ. Flexible thin-film black gold membranes with ultrabroadband plasmonic nanofocusing for efficient solar vapour generation. Nat Commun 2015;6:10103.
[9] Bait O. Exergy, environ–economic and economic analyses of a tubular solar water heater assisted solar still. J Cleaner Prod 2019;212:630–46.
[10] Bait O, Si-Ameur M. Enhanced heat and mass transfer in solar stills using nanofluids: a review. Sol Energy 2018;170:694–722.
[11] Berkessa YW, Lang Q, Yan B, Kuang S, Mao D, Shu L, et al. Anion exchange membrane organic fouling and mitigation in salt valorization process from high salinity textile wastewater by bipolar membrane electrodialysis. Desalination 2019;465:94–103.
[12] Chafidz A, Kerme ED, Wazeer I, Khalid Y, Ajbar A, Al-Zahrani SM. Design and fabrication of a portable and hybrid solar-powered membrane distillation system. J Cleaner Prod 2016;133:631–47.
[13] Cuce E, Cuce PM, Saxena A, Guclu T, Besir AB. Performance analysis of a novel solar desalination system – Part 1: The unit with sensible energy storage and booster reflector without thermal insulation and cooling system. Sustainable Energy Technol Assess 2020;37:100566. https://doi.org/10.1016/j.seta.2019.100566.
[14] Dashtban M, Tabrizi FF. Thermal analysis of a weir-type cascade solar still integrated with PCM storage. Desalination 2011;279(1-3):415–22.
[15] Dev R, Abdul-Wahab SA, Tiwari GN. Performance study of the inverted absorber solar still with water depth and total dissolved solid. Appl Energy 2011;88(1):252–64.
[16] Dhindsa GS, Mittal MK. Experimental study of basin type vertical multiple effect diffusion solar still integrated with mini solar pond to generate nocturnal distillate. Energy Convers Manage 2018;165:669–80.
[17] Dumka P, Chauhan R, Mishra DR. Experimental and theoretical evaluation of a conventional solar still augmented with jute covered plastic balls. J Storage Mater 2020;32:101874. https://doi.org/10.1016/j.est.2020.101874.
[18] Dumka P, Kushwah Y, Sharma A, Mishra DR. Comparative analysis and experimental evaluation of single slope solar still augmented with permanent magnets and conventional solar still. Desalination 2019;459:34–45.
[19] El-Bialy E, Shalaby SM, Kabeel AE, Fathy AM. Cost analysis for several solar desalination systems. Desalination 2016;384:12–30.
[20] El-Sebaii AA, El-Bialy E. Advanced designs of solar desalination systems: a review. Renew Sustain Energy Rev 2015;49:1198–212.
[21] Elaziz MA, Elsheikh AH, Sharshir SW. Improved prediction of oscillatory heat transfer coefficient for a thermoacoustic heat exchanger using modified adaptive neuro-fuzzy inference system. Int J Refrig 2019;102:47–54.
[22] Elbar ARA, Yousef MS, Hassan H. Energy, exergy, exergoeconomic and enviroeconomic (4E) evaluation of a new integration of solar still with photovoltaic panel. J Cleaner Prod 2019;233:665–80.
[23] Elmaadawy K, Elaziz MA, Elsheikh AH, Moawad A, Liu B, Lu S. Utilization of random vector functional link integrated with manta ray foraging optimization for effluent prediction of wastewater treatment plant. J Environ Manage 2021;298:113520. https://doi.org/10.1016/j.jenvman.2021.113520.
[24] Elsheikh AH, Abd Elaziz M, Ramesh B, Egiza M, Al-qaness MAA. Modeling of drilling process of GFRP composite using a hybrid random vector functional link network/parasitism-predation algorithm. J Mater Res Technol 2021;14:298–311.
[25] Elsheikh AH, Abd Elaziz M, Vendan A. Modeling ultrasonic welding of polymers using an optimized artificial intelligence model using a gradient-based optimizer. Weld World 2021.
[26] Elsheikh AH, Elaziz MA, Das SR, Muthuramalingam T, Lu S. A new optimized predictive model based on political optimizer for eco-friendly MQL-turning of AISI 4340 alloy with nano-lubricants. J Manuf Processes 2021;67:562–78.
[27] Elsheikh AH, Katekar VP, Muskens OL, Deshmukh SS, Elaziz MA, Dabour SM. Utilization of LSTM neural network for water production forecasting of a stepped solar still with a corrugated absorber plate. Process Saf Environ Prot 2021;148:273–82.
[28] Elsheikh AH, Muthuramalingam T, Shanmugan S, Mahmoud Ibrahim AM, Ramesh B, Khoshaim AB, et al. Fine-tuned artificial intelligence model using pigeon optimizer for prediction of residual stresses during turning of Inconel 718. J Mater Res Technol 2021;15:3622–34.
[29] Elsheikh AH, Sharshir SW, Abd Elaziz M, Kabeel AE, Guilan W, Haiou Z. Modeling of solar energy systems using artificial neural network: a comprehensive review. Sol Energy 2019;180:622–39.
[30] Elsheikh AH, Sharshir SW, Ahmed Ali MK, Shaibo J, Edreis EMA, Abdelhamid T, et al. Thin film technology for solar steam generation: A new dawn. Sol Energy 2019;177:561–75.
[31] Elsheikh AH, Sharshir SW, Kabeel AE, Sathyamurthy R. Application of Taguchi method to determine the optimal water depth and glass cooling rate in solar stills. Scientia Iranica 2021;28(2):731–42.
[32] Elsheikh AH, Sharshir SW, Mostafa ME, Essa FA, Ahmed Ali MK. Applications of nanofluids in solar energy: a review of recent advances. Renew Sustain Energy Rev 2018;82:3483–502.
[33] Elsheikh AH, Shehabeldeen TA, Zhou J, Showaib E, Abd Elaziz M. Prediction of laser cutting parameters for polymethylmethacrylate sheets using random vector functional link network integrated with equilibrium optimizer. J Intell Manuf 2021;32(5):1377–88.
[34] Essa FA, Abd Elaziz M, Elsheikh AH. An enhanced productivity prediction model of active solar still using artificial neural network and Harris Hawks optimizer. Appl Therm Eng 2020;170:115020. https://doi.org/10.1016/j.applthermaleng.2020.115020.
[35] Essa FA, Elsheikh AH, Algazzar AA, Sathyamurthy R, Ahmed Ali MK, Elaziz MA, et al. Eco-friendly coffee-based colloid for performance augmentation of solar stills. Process Saf Environ Prot 2020;136:259–67.
[36] Essa FA, Elsheikh AH, Sathyamurthy R, Muthu Manokar A, Kandeal AW, Shanmugan S, et al. Extracting water content from the ambient air in a double-slope half-cylindrical basin solar still using silica gel under Egyptian conditions. Sustainable Energy Technol Assess 2020;39:100712. https://doi.org/10.1016/j.seta.2020.100712.
[37] Essa FA, Omara ZM, Abdullah AS, Shanmugan S, Panchal H, Kabeel AE, et al. Wall-suspended trays inside stepped distiller with Al2O3/paraffin wax mixture and vapor suction: experimental implementation. J Storage Mater 2020;32:102008. https://doi.org/10.1016/j.est.2020.102008.
[38] Fang J, Liu Q, Zhang W, Gu J, Su Y, Su H, et al. Ag/diatomite for highly efficient solar vapor generation under one-sun irradiation. J Mater Chem A 2017;5(34):17817–21.
[39] Fath HES, El-Samanoudy M, Fahmy K, Hassabou A. Thermal-economic analysis and comparison between pyramid-shaped and single-slope solar still configurations. Desalination 2003;159(1):69–79.
[40] Feilizadeh M, Estahbanati MRK, Khorram M, Rahimpour MR. Experimental investigation of an active thermosyphon solar still with enhanced condenser. Renewable Energy 2019;143:328–34.
[41] Ghasemi H, Ni G, Marconnet AM, Loomis J, Yerci S, Miljkovic N, et al. Solar steam generation by heat localization. Nat Commun 2014;5(1). https://doi.org/10.1038/ncomms5449.
[42] Hamdan M, Khalil HR, Abdelhafez E. Comparison of neural network models in the estimation of the performance of solar still under jordanian climate. J Clean Energy Technol 2013;1(3):238–42.
[43] Hammadi SH. Integrated solar still with an underground heat exchanger for clean water production. J King Saud Univ - Eng Sci 2019;32(5):339–45.
[44] Hao D, Yang Y, Xu B, Cai Z. Bifunctional fabric with photothermal effect and photocatalysis for highly efficient clean water generation. ACS Sustainable Chem Eng 2018.
[45] Higgins MW, Shakeel Rahmaan AR, Devarapalli RR, Shelke MV, Jha N. Carbon fabric based solar steam generation for waste water treatment. Sol Energy 2018;159:800–10.
[46] Holman JP, Gajda WJ. Experimental methods for engineers. McGraw-Hill New York; 2001.
[47] Huang J, He Y, Wang L, Huang Y, Jiang B. Bifunctional Au@TiO2 core–shell nanoparticle films for clean water generation by photocatalysis and solar evaporation. Energy Convers Manage 2017;132:452–9.
[48] Huang J, Jin T, Liang M, Chen H. Prediction of heat exchanger performance in cryogenic oscillating flow conditions by support vector machine. Appl Therm Eng 2021;182:116053. https://doi.org/10.1016/j.applthermaleng.2020.116053.
[49] Jia J, Liang W, Sun H, Zhu Z, Wang C, Li A. Fabrication of bilayered attapulgite for solar steam generation with high conversion efficiency. Chem Eng J 2019;361:999–1006.
[50] Kabeel AE, Abdelgaied M. Enhancement of pyramid-shaped solar stills performance using a high thermal conductivity absorber plate and cooling the glass cover. Renewable Energy 2019;146:769–75.
[51] Kabeel AE, Hamed AM, El-Agouz SA. Cost analysis of different solar still configurations. Energy 2010;35(7):2901–8.

[52] Kabeel AE, Khairat Dawood MM, Ramzy K, Nabil T, Elnaghi B, Elkassar A. Enhancement of single solar still integrated with solar dishes: an experimental approach. Energy Convers Manag 2019;196:165–74.
[53] Kabeel AE, Teamah MA, Abdelgaied M, Abdel Aziz GB. Modified pyramid solar still with v-corrugated absorber plate and PCM as a thermal storage medium. J Cleaner Prod 2017;161:881–7.
[54] Kalidasa Murugavel K, Sivakumar S, Riaz Ahamed J, Chockalingam KKSK, Srithar K. Single basin double slope solar still with minimum basin depth and energy storing materials. Appl Energy 2010;87(2):514–23.
[55] Kashyap V, Al-Bayati A, Sajadi SM, Irajizad P, Wang SH, Ghasemi H. A flexible anti-clogging graphite film for scalable solar desalination by heat localization. J Mater Chem A 2017;5(29):15227–34.
[56] Kaur M, Ishii S, Shinde SL, Nagao T. All-ceramic microfibrous solar steam generator: TiN plasmonic nanoparticle-loaded transparent microfibers. ACS Sustainable Chem Eng 2017;5(10):8523–8.
[57] Ketabchi F, Gorjian S, Sabzehparvar S, Shadram Z, Ghoreishi MS, Rahimzadeh H. Experimental performance evaluation of a modified solar still integrated with a cooling system and external flat-plate reflectors. Sol Energy 2019;187:137–46.
[58] Khoshaim AB, Elsheikh AH, Moustafa EB, Basha M, Mosleh AO. Prediction of residual stresses in turning of pure iron using artificial intelligence-based methods. J Mater Res Technol 2021;11:2181–94.
[59] Kumar R, Agrawal HP, Shah A, Bansal HO. Maximum power point tracking in wind energy conversion system using radial basis function based neural network control strategy. Sustainable Energy Technol Assess 2019;36:100533. https://doi.org/10.1016/j.seta.2019.100533.
[60] Leijon J, Boström C. Freshwater production from the motion of ocean waves – A review. Desalination 2018;435:161–71.
[61] Li T, Liu H, Zhao X, Chen G, Dai J, Pastel G, et al. Scalable and highly efficient mesoporous wood-based solar steam generation device: localized heat, rapid water transport. Adv Funct Mater 2018;28(16):1707134. https://doi.org/10.1002/adfm.v28.1610.1002/adfm.201707134.
[62] Li X, Xu W, Tang M, Zhou L, Zhu B, Zhu S, et al. Graphene oxide-based efficient and scalable solar desalination under one sun with a confined 2D water path. PNAS 2016;113(49):13953–8.
[63] Li Y, Gao T, Yang Z, Chen C, Kuang Y, Song J, et al. Graphene oxide-based evaporator with one-dimensional water transport enabling high-efficiency solar desalination. Nano Energy 2017;41:201–9.
[64] Zhang L, Tang B, Wu J, Li R, Wang P. Hydrophobic light-to-heat conversion membranes with self-healing ability for interfacial solar heating. Adv Mater 2015;27(33):4889–94.
[65] Liu K-K, Jiang Q, Tadepalli S, Raliya R, Biswas P, Naik RR, et al. Wood-graphene oxide composite for highly efficient solar steam generation and desalination. ACS Appl Mater Interfaces 2017;9(8):7675–81.
[66] Liu S, Huang C, Luo X, Guo C. Performance optimization of bi-layer solar steam generation system through tuning porosity of bottom layer. Appl Energy 2019;239:504–13.
[67] Liu X, Hou B, Wang G, Cui Z, Zhu X, Wang X. Black titania/graphene oxide nanocomposite films with excellent photothermal property for solar steam generation. J Mater Res 2018;33(6):674–84.
[68] Liu Y, Chen J, Guo D, Cao M, Jiang L. Floatable, self-cleaning, and carbon-black-based superhydrophobic gauze for the solar evaporation enhancement at the air-water interface. ACS Appl Mater Interfaces 2015;7(24):13645–52.
[69] Luo X, Wu D, Huang C, Rao Z. Skeleton double layer structure for high solar steam generation. Energy 2019;183:1032–9.
[70] Ma S, Qarony W, Hossain MI, Yip CT, Tsang YH. Metal-organic framework derived porous carbon of light trapping structures for efficient solar steam generation. Sol Energy Mater Sol Cells 2019;196:36–42.
[71] Mashaly AF, Alazba AA. Thermal performance analysis of an inclined passive solar still using agricultural drainage water and artificial neural network in arid climate. Sol Energy 2017;153:383–95.
[72] Motahar S, Bagheri-Esfeh H. Artificial neural network based assessment of grid-connected photovoltaic thermal systems in heating dominated regions of Iran. Sustainable Energy Technol Assess 2020;39:100694. https://doi.org/10.1016/j.seta.2020.100694.
[73] Ni G, Li G, Boriskina Svetlana V, Li H, Yang W, Zhang T, Chen G. Steam generation under one sun enabled by a floating structure with thermal concentration. Nat Energy 2016;1:16126.
[74] Ortega-Delgado B, Giacalone F, Catrini P, Cipollina A, Piacentino A, Tamburini A, et al. Reverse electrodialysis heat engine with multi-effect distillation: exergy analysis and perspectives. Energy Convers Manage 2019;194:140–59.
[75] Ortega-Delgado B, Palenzuela P, Alarcón-Padilla D-César. Parametric study of a multi-effect distillation plant with thermal vapor compression for its integration into a Rankine cycle power block. Desalination 2016;394:18–29.
[76] PK N, El-Agouz SA, DG HS, M E, B M, D Mb, Sathyamurthy R, R B. Analysis of an inclined solar still with baffles for improving the yield of fresh water. Process Saf Environ Prot 2017;105:326–37.
[77] Patra H, Adhikari SK, Kunar S. Groundwater prospecting and management. Springer; 2016.
[78] Petela R. Exergy of undiluted thermal radiation. Sol Energy 2003;74(6):469–88.
[79] Jiang Q, Tian L, Liu K-K, Tadepalli S, Raliya R, Biswas P, et al. Bilayered biofoam for highly efficient solar steam generation. Adv Mater 2016;28(42):9400–7.
[80] Rahmani A, Boutriaa A. Numerical and experimental study of a passive solar still integrated with an external condenser. Int J Hydrogen Energy 2017;42(48):29047–55.
[81] Rajaseenivasan T, Murugavel K. Theoretical and experimental investigation on double basin double slope solar still. Desalination 2013;319:25–32.
[82] Sahle-Demessie E, Aly Hassan A, El Badawy A. Bio-desalination of brackish and seawater using halophytic algae. Desalination 2019;465:104–13.
[83] Sahota L, Tiwari GN. Effect of Al2O3 nanoparticles on the performance of passive double slope solar still. Sol Energy 2016;130:260–72.
[84] Santos NI, Said AM, James DE, Venkatesh NH. Modeling solar still production using local weather data and artificial neural networks. Renewable Energy 2012;40(1):71–9.
[85] Sathyamurthy R, Harris Samuel DG, Nagarajan PK. Theoretical analysis of inclined solar still with baffle plates for improving the fresh water yield. Process Saf Environ Prot 2016;101:93–107.
[86] Selvaraj K, Natarajan A. Factors influencing the performance and productivity of solar stills - A review. Desalination 2018;435:181–7.
[87] Shafieian A, Rizwan Azhar M, Khiadani M, Kanti Sen T. Performance improvement of thermal-driven membrane-based solar desalination systems using nanofluid in the feed stream. Sustainable Energy Technol Assess 2020;39:100715. https://doi.org/10.1016/j.seta.2020.100715.
[88] Sharan P, Neises T, Turchi C. Optimal feed flow sequence for multi-effect distillation system integrated with supercritical carbon dioxide Brayton cycle for seawater desalination. J Cleaner Prod 2018;196:889–901.
[89] Sharshir SW, Ellakany YM, Algazzar AM, Elsheikh AH, Elkadeem MR, Edreis EMA, et al. A mini review of techniques used to improve the tubular solar still performance for solar water desalination. Process Saf Environ Prot 2019;124:204–12.
[90] Sharshir SW, Elsheikh AH, Ellakany YM, Kandeal AW, Edreis EMA, Sathyamurthy R, et al. Improving the performance of solar still using different heat localization materials. Environ Sci Pollut Res 2020;27(11):12332–44.
[91] Sharshir SW, Elsheikh AH, Peng G, Yang N, El-Samadony MOA, Kabeel AE. Thermal performance and exergy analysis of solar stills – A review. Renew Sustain Energy Rev 2017;73:521–44.
[92] Sharshir SW, Peng G, Elsheikh AH, Edreis EMA, Eltawil MA, Abdelhamid T, et al. Energy and exergy analysis of solar stills with micro/nano particles: a comparative study. Energy Convers Manage 2018;177:363–75.
[93] Sharshir SW, Peng G, Elsheikh AH, Eltawil MA, Elkadeem MR, Dai H, et al. Influence of basin metals and novel wick-metal chips pad on the thermal performance of solar desalination process. J Cleaner Prod 2020;248:119224. https://doi.org/10.1016/j.jclepro.2019.119224.
[94] Sharshir SW, Peng G, Wu L, Yang N, Essa FA, Elsheikh AH, et al. Enhancing the solar still performance using nanofluids and glass cover cooling: experimental study. Appl Therm Eng 2017;113:684–93.
[95] Srithar K, Rajaseenivasan T. Performance analysis on a solar bubble column humidification dehumidification desalination system. Process Saf Environ Prot 2017;105:41–50.
[96] Sun Y, Gao J, Liu Y, Kang H, Xie M, Wu F, et al. Copper sulfide-macroporous polyacrylamide hydrogel for solar steam generation. Chem Eng Sci 2019;207:516–26.
[97] Suneesh PU, Jayaprakash R, Arunkumar T, Denkenberger D. Effect of air flow on "V" type solar still with cotton gauze cooling. Desalination 2014;337:1–5.
[98] Taner T. Optimisation processes of energy efficiency for a drying plant: a case of study for Turkey. Appl Therm Eng 2015;80:247–60.
[99] Taner T. Energy and exergy analyze of PEM fuel cell: a case study of modeling and simulations. Energy 2018;143:284–94.
[100] Taner T. The novel and innovative design with using H2 fuel of PEM fuel cell: Efficiency of thermodynamic analyze. Fuel 2021;302:121109. https://doi.org/10.1016/j.fuel.2021.121109.
[101] Taner T, Naqvi SAH, Ozkaymak M. Techno-economic analysis of a more efficient hydrogen generation system prototype: a case study of PEM electrolyzer with Cr-C coated SS304 bipolar plates. Fuel Cells 2019;19(1):19–26.
[102] Taner T, Sivrioglu M. A techno-economic & cost analysis of a turbine power plant: a case study for sugar plant. Renew Sustain Energy Rev 2017;78:722–30.
[103] Topal H, Taner T, Naqvi SAH, Altınsoy Y, Amirabedin E, Ozkaymak M. Exergy analysis of a circulating fluidized bed power plant co-firing with olive pits: a case study of power plant in Turkey. Energy 2017;140:40–6.
[104] Velmurugan V, Naveen Kumar KJ, Noorul Haq T, Srithar K. Performance analysis in stepped solar still for effluent desalination. Energy 2009;34(9):1179–86.
[105] Wang X, He Y, Liu X, Cheng G, Zhu J. Solar steam generation through bio-inspired interface heating of broadband-absorbing plasmonic membranes. Appl Energy 2017;195:414–25.
[106] Wu B, Maleki A, Pourfayaz F, Rosen MA. Optimal design of stand-alone reverse osmosis desalination driven by a photovoltaic and diesel generator hybrid system. Sol Energy 2018;163:91–103.
[107] Xiong J, Xie G, Zheng H. Experimental and numerical study on a new multi-effect solar still with enhanced condensation surface. Energy Convers Manage 2013;73:176–85.
[108] Wu X, Chen GY, Zhang W, Liu X, Xu H. A plant-transpiration-process-inspired strategy for highly efficient solar evaporation. Adv Sustainable Syst 2017;1(6):1700046. https://doi.org/10.1002/adsu.v1.610.1002/adsu.201700046.
[109] Xue G, Liu K, Chen Q, Yang P, Li J, Ding T, et al. Robust and low-cost flame-treated wood for high-performance solar steam generation. ACS Appl Mater Interfaces 2017;9(17):15052–7.
[110] Liu Y, Yu S, Feng R, Bernard A, Liu Y, Zhang Y, et al. A bioinspired, reusable, paper-based system for high-performance large-scale evaporation. Adv Mater 2015;27(17):2768–74.
[111] Yao M, Woo YC, Tijing LD, Choi J-S, Shon HK. Effects of volatile organic compounds on water recovery from produced water via vacuum membrane distillation. Desalination 2018;440:146–55.

[112] Ito Y, Tanabe Y, Han J, Fujita T, Tanigaki K, Chen M. Multifunctional porous graphene for high-efficiency steam generation by heat localization. Adv Mater 2015;27(29):4302–7.

[113] Yousef MS, Hassan H. An experimental work on the performance of single slope solar still incorporated with latent heat storage system in hot climate conditions. J Cleaner Prod 2019;209:1396–410.

[114] Yu S, Zhang Y, Duan H, Liu Y, Quan X, Tao P, et al. The impact of surface chemistry on the performance of localized solar-driven evaporation system. Sci Rep 2015;5(1). https://doi.org/10.1038/srep13600.

[115] Zanganeh P, Goharrizi AS, Ayatollahi S, Feilizadeh M. Productivity enhancement of solar stills by nano-coating of condensing surface. Desalination 2019;454:1–9.

[116] Zhang X-F, Wang Z, Song L, Feng Y, Yao J. Chinese ink enabled wood evaporator for continuous water desalination. Desalination 2020;496:114727. https://doi.org/10.1016/j.desal.2020.114727.

[117] Guo Z, Ming X, Wang G, Hou B, Liu X, Mei T, et al. Super-hydrophilic copper sulfide films as light absorbers for efficient solar steam generation under one sun illumination. Semicond Sci Technol 2018;33(2):025008. https://doi.org/10.1088/1361-6641/aaa323.

[118] Zhou L, Tan Y, Wang J, Xu W, Yuan Y, Cai W, et al. 3D self-assembly of aluminium nanoparticles for plasmon-enhanced solar desalination. Nat Photonics 2016;10(6):393–8.

[119] Zhu G, Xu J, Zhao W, Huang F. Constructing black titania with unique nanocage structure for solar desalination. ACS Appl Mater Interfaces 2016;8(46):31716–21.